Available online at www.eccomasproceedia.org
Eccomas Proceedia SMART (2023) 1669-1680

ECCOMAS
Proceedia

X ECCOMAS Thematic Conference on Smart Structures and Materials
SMART 2023
D.A. Saravanos, A. Benjeddou, N. Chrysochoidis and T. Theodosiou (Eds)

TOPOLOGY OPTIMIZATION-BASED DESIGN OF A SENSOR-INTEGRATING FEATHER KEY

STEPHANIE SELTMANN*, BENJAMIN MUHAMMEDI* AND ALEXANDER HASSE*

*Chemnitz University of Technology
Professorship Machine Elements and Product Development
09107 Chemnitz, Germany
e-mail: stephanie.seltmann@mb.tu-chemnitz.de, web page: https://www.tu-chemnitz.de/mb/mp/

Abstract. Feather keys are used to connect shafts and hubs and transmit torques. By adding sensors to the feather key, the torques applied via its deformation can be recorded. However, the feather key is subject to non-uniform surface pressure, causing complex deformation. Typically, a large number of strain gauges are required to measure this deformation, and complex calculations are needed to determine the resulting circumferential force. But by optimizing the eigenbehavior of the feather key through topology optimization, its geometry can be adapted so that it always deforms according to a linear combination of a few desired deformation modes, regardless of surface pressure. This greatly reduces the number of strain gauges needed to measure the deformation state, making it easier to determine the circumferential force. The resulting geometry is tested under realistic conditions, and the study shows that the desired properties can be achieved with the use of two strain gauges.

Key words: shaft hub connection, feather key, topology optimization, sensor integrating machine element, compliant mechanism

1 INTRODUCTION

In a feather key connection, the feather key establishes the form fit between the shaft and hub so that torques can be transmitted. Since it transmits the torques directly, the feather key is particularly suitable for in-situ measurements. For this reason, it makes sense to enhance the feather key with sensors to record the torques applied to the shaft-hub connection via the deformation of the feather key. Such enhanced machine elements are commonly referred to as sensing design elements [1]. Currently, such an extension is being researched for quite a few machine elements. However, the literature specifically for sensor-integrating feather keys is still sparse. A concept study [2] shows, among other aspects, special design requirements for sensor integration using the example of the feather key connection. In doing so, this study points out that in sensor integration, the fits between the components of the connections can have a major impact on the measurement results. In addition, the torque transmitted during

Peer-review under responsibility of the organizing committee of SMART 2023.
doi: 10.7712/150123.9938.451778

operation creates a surface pressure on the feather key, which causes complex deformation. For the back calculation to the transmitted torque, the resulting deformation must be completely recorded. For this purpose, theoretically an infinite number of strain gauges would have to be placed on the feather key. In order to improve the measurability of the deformation, the shape of the feather key, which is normally precisely defined via DIN 6885 [3], was changed in two different patents. This creates areas in the feather key cross-section where defined deformation patterns with strong deformations are present. In these areas, the strain is measured with the aid of a few sensors and the transmitted torque is calculated from this. Thus, similar to a load cell, the feather key functions directly as a force sensor by means of a defined deformation. In patent [4], the shape of the feather key is modified so that the torque can be determined by measuring a bending deformation. In patent [5], recesses are made in the cross-section of the feather key that exhibit measurable deformations when a certain load is exceeded. The geometries needed to improve the measurability of the deformation are often determined by classical design methods. Here, however, the results depend on the experience of the designer.

Another possibility for finding possible geometries is topology optimization. Here, material is distributed in a defined design space in a certain way so that an objective function is optimized and certain restrictions are observed. In the topology optimization of compliant mechanisms (CM), the objective is the same as for the sensor-integrating feather key: A structure is designed to deform according to defined deformation patterns. CM show similarities to conventional mechanisms: While conventional mechanisms realize the desired deformation by the relative motion of rigid links to each other, which are connected with ideal joints, CMs realize this with the help of elastic deformation. The number of independent coordinates needed to define a configuration of a conventional mechanism is called mobility. This quantity cannot be readily applied to CM. However, there is a quantity that is similar to it: the pseudo-mobility m. This specifies for how many independent desired deformation patterns a CM is designed [6]. During optimization, the desired motion and defined load cases are imposed on so-called input and output degrees of freedom (input and output DoFs). For topology optimization of CM with pseudo-mobility one, there are many well-known optimization formulations. Here, the CMs are optimized to produce desired deformations for certain defined load cases. A comparison of the best known formulations for the case of small displacements can be found in [7]. However, when designing force sensors such as the compliant feather key, designing CM for a pseudo-mobility greater than one may be more favorable. Here, however, the number of known optimization approaches is small. In [8], a "grip-and-move manipulator" is designed. For this, a multi-objective optimization is used, where the size of the working space and the maximum movement of the output DoFs in a desired direction are optimized. In [9], an objective function is maximized which includes the weighted sum of displacements caused by given forces. The approach is tested on CM with pseudo-mobility of two and three. The objective function in [10] involves the ratio of a total mutual potential energy (measure of structural flexibility) to strain energy (measure of structural stiffness) and is maximized. This approach is tested on a CM with a pseudo-mobility of two. Alonso [11] maximizes the mutual potential energy to design a mechanism that combines a crunching mechanism and an inverter mechanism.

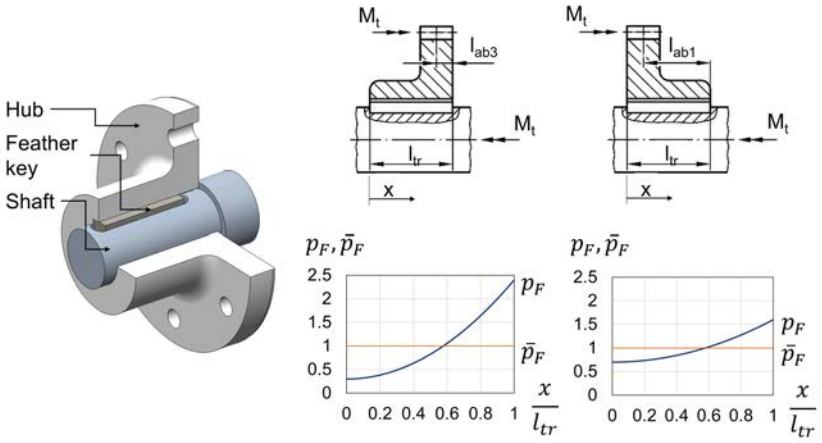

Figure 1: Schematic representation of a feather key connection and the surface pressure distribution p_F for different geometries of the hub at the same torque M_t over the feather key length.

Despite the different objective functions, the presented approaches have the following similarities: On the one hand, CMs are designed for a small number of output DoFs, and on the other hand, synthesis is performed for defined load cases at the input and output DoFs. These approaches are not suitable for the design of a sensor-integrating feather key for the following reasons: Depending on the shaft and hub geometry as well as the load input and output, different surface pressure distributions are usually applied to a feather key. Some characteristic surface pressure distributions p_F over the feather key length l_{tr} depending on the hub shape are shown in Figure 1. Since the applied torque M_t is the same, the mean value of the pressure distributions over the feather key length $\bar{p}_F$ is the same in each case. It can be seen, first, that many input and output DoFs are needed to apply the complex pressure fields for optimization. A second limitation is that the shape of the pressure fields varies. Thus, due to the load case dependent design, a new feather key with optimal characteristics would have to be designed or the existing feather key would have to be recalibrated each time the geometry of the assembly changes. These limitations are circumvented by an optimization algorithm co-developed by two of the authors of this paper: the modal approach. By optimizing the eigenbehavior of the structure, a CM can be designed for the case of small displacements that always deforms with a linear combination of the same set of m deformation patterns (hereafter referred to as modes), regardless of the applied load. This new class of CM is called CM with selective compliance [12]. In addition, the approach is suitable for the synthesis of CM with many input and output DoFs. By optimizing the topology of the feather key with the modal approach, it then always deforms according to a linear combination of a small number of m equal modes for different pressure distributions. In order to accurately determine this deformation, an infinite number of strain gauges are no longer required, in contrast to the non-optimized feather key. Only m strain gauges are needed, which do not have to be recalibrated when boundary conditions change. This greatly simplifies both the measurement task and the back calculation to the transmitted torque.

2 METHOD FOR STIFFNESS CONDITIONING OF THE FEATHER KEY

2.1 DESIGN PROBLEM

As explained earlier, the feather key is to be optimized as CM with selective compliance and multiple pseudo-mobility. As such, it must have characteristic properties [6], which are briefly described below. The DoFs of the structure to be optimized are discretized to p DoFs. For CM with selective compliance, the DoFs no longer need to be divided into input and output DoFs. They are grouped here as q active DoFs a. External forces act on them and they produce a desired deformation. All $p-q$ other DoFs of the structure are called passive DoFs c. Under these conditions, the stiffness matrix $\mathbf{K}$, the displacement vector $\mathbf{u}$ and the force vector $\mathbf{F}$ can be subdivided as follows and the stiffness matrix $\mathbf{K}$ can be condensed to its active DoFs ($\bar{\mathbf{K}}$):

$$\mathbf{K}\mathbf{u} = \mathbf{f} \iff \begin{bmatrix} \mathbf{K}_{aa} & \mathbf{K}_{ac} \\ \mathbf{K}_{ca} & \mathbf{K}_{cc} \end{bmatrix} \begin{bmatrix} \mathbf{u}_a \\ \mathbf{u}_c \end{bmatrix} = \begin{bmatrix} \mathbf{f}_a \\ \mathbf{0} \end{bmatrix} \tag{1}$$

$$(\mathbf{K}_{aa} - \mathbf{K}_{ac}\mathbf{K}_{cc}^{-1}\mathbf{K}_{ca})\mathbf{u}_a = \bar{\mathbf{K}}\mathbf{u}_a = \mathbf{f}_a \tag{2}$$

From $\bar{\mathbf{K}}$ the eigenvalues $\lambda_j, j = 1...q$ and eigenmodes $\bar{\boldsymbol{\chi}}_j, j = 1...q$ are calculated using the following eigenvalue problem:

$$\bar{\mathbf{K}}\bar{\boldsymbol{\chi}} = \lambda\bar{\boldsymbol{\chi}} \tag{3}$$

The eigenmodes specify all possible deformation patterns that compose the deformation of the CM when forces act on the active DoFs. Here we divide the eigenmodes into the set of desired (kinematic) $\bar{\mathbf{X}}_d$ and undesired (parasitic) $\bar{\mathbf{X}}_{ud}$ eigenmodes:

$$\bar{\mathbf{X}} = \begin{bmatrix} \bar{\mathbf{X}}_d & | & \bar{\mathbf{X}}_{ud} \end{bmatrix}; \; \bar{\mathbf{X}}_d = \begin{bmatrix} \bar{\boldsymbol{\chi}}_1 & \bar{\boldsymbol{\chi}}_2 & \cdots & \bar{\boldsymbol{\chi}}_m \end{bmatrix}; \; \bar{\mathbf{X}}_{ud} = \begin{bmatrix} \bar{\boldsymbol{\chi}}_{m+1} & \bar{\boldsymbol{\chi}}_{m+2} & \cdots & \bar{\boldsymbol{\chi}}_q \end{bmatrix}; \tag{4}$$

The kinematic eigenmodes are the deformation patterns according to which the CM should deform under any load at the active DoFs. Parasitic eigenmodes describe deformation patterns that should, as far as possible, not occur regardless of the type of loading. Under the assumption that

$$\bar{\boldsymbol{\chi}}_i^T\bar{\boldsymbol{\chi}}_i = 1, \; i = 1...q \tag{5}$$

holds, the primary stiffness $K_{pi}(\bar{\mathbf{K}})$ and secondary stiffness $K_s(\bar{\mathbf{K}})$ of the CM can be calculated:

$$K_{pi}(\bar{\mathbf{K}}) = \lambda_i = \bar{\boldsymbol{\chi}}_i^T\bar{\mathbf{K}}\bar{\boldsymbol{\chi}}_i, \; i = 1 \dots m \tag{6}$$

$$K_s(\bar{\mathbf{K}}) = \lambda_{\bar{\boldsymbol{\chi}}_{m+1}} = \bar{\boldsymbol{\chi}}_{m+1}^T\bar{\mathbf{K}}\bar{\boldsymbol{\chi}}_{m+1} \tag{7}$$

The primary stiffnesses are the eigenvalues assigned to the kinematic eigenmodes. The secondary stiffness is the smallest eigenvalue of the parasitic eigenmodes. The eigenvalues are a measure of the strain energy required to deform a CM according to the associated eigenmode normalized with condition (5). If the eigenvalues are close, the CM will always deform using a linear combination of all eigenmodes. However, if the CM is designed as a CM with selective compliance, the eigenmode is optimized so that the primary stiffness is much smaller than

the secondary stiffness. The ratio of secondary stiffness to largest primary stiffness is called selectivity:

$$S = \lambda_{m+1}/\lambda_m \tag{8}$$

If this is sufficiently large, the deformation $\bar{\mathbf{u}}_d$ of the active DoFs of the CM with selective compliance will be approximately composed of the set of kinematic eigenmodes regardless of the applied loads:

$$\bar{\mathbf{u}}_d = \alpha_1 \cdot \bar{\boldsymbol{\chi}}_1 + \alpha_2 \cdot \bar{\boldsymbol{\chi}}_2 + \ldots + \alpha_m \cdot \bar{\boldsymbol{\chi}}_m \tag{9}$$

The scaling factors α possess the dimension of length. Thus, a high selectivity is an optimization goal. Furthermore, the kinematic eigenmodes are to be determined during the optimization. For this purpose, a set of desired deformation modes $\bar{\boldsymbol{\Phi}} = [\bar{\boldsymbol{\varphi}}_1, \bar{\boldsymbol{\varphi}}_2, \ldots, \bar{\boldsymbol{\varphi}}_m]$ is given to the optimization. These then span the space of desired deformation modes $\mathbb{K}^{\bar{\Phi}}$. Since they represent a vector base, they must be orthonormal to each other:

$$\left.\begin{array}{l} \bar{\boldsymbol{\varphi}}_i^T \bar{\boldsymbol{\varphi}}_j = 1,\ i = j \\ \bar{\boldsymbol{\varphi}}_i^T \bar{\boldsymbol{\varphi}}_j = 0,\ i \neq j \end{array}\right\}, i = 1...m,\ j = 1...m \tag{10}$$

The second optimization objective is thus to ensure that the kinematic eigenmodes of the CM $\bar{\mathbf{X}}_d$ with selective compliance span approximately the same subspace as the set of desired deformation modes. If these two optimization objectives are achieved for the stiffness-conditioned feather key, its deformation will always be composed of m desired deformation modes regardless of the applied pressure distribution, and both m and the desired deformation modes can be chosen by the designer for the optimization algorithm presented below.

2.2 OPTIMIZATION FORMULATION

To achieve the goals mentioned in the previous section, the optimization procedure presented in [6] is used. For this, first a design space is defined, which is filled with r finite elements. Usually, 4-node quadrilateral elements with full integration are used. Each finite element has a constant element stiffness matrix $\mathbf{K}_i$, whose stiffness is scaled with a design variable x_i before fitting into the overall stiffness matrix:

$$\mathbf{K}(\mathbf{x}) = \sum_{i=1}^{r} x_i \mathbf{K}_i \tag{11}$$

The stiffness matrix established using equation (11) is then condensed to its active DoFs using equation (2). The following optimization problem must be solved for this stiffness matrix:

$$\max\ f(\mathbf{x}) = K_s(\bar{\mathbf{K}}) \tag{12}$$

s.t.:

$$g_i(\mathbf{x}) = \bar{\boldsymbol{\varphi}}_i^T \bar{\mathbf{K}} \bar{\boldsymbol{\varphi}}_i - 2\mu \leq 0, i = 1 \dots m \tag{13}$$

$$m(\mathbf{x}) = \sum_{i=0}^{r} x_i^{1/\eta} - rV \leq 0 \tag{14}$$

$$x_i^l \leq x_i \leq x_i^u, i = 1...r \tag{15}$$

High selectivity can be achieved indirectly by increasing the secondary stiffness $K_s(\bar{\mathbf{K}})$ of the CM in equation (12), while corresponding expressions for the primary stiffnesses are constrained to a fixed value μ in (13). Equation (14) constraints the volume of the structure to a constant value V. Here, a penalty factor η is introduced to obtain as optimization result design variables that take either a value close to zero or a value close to one [13]. Equation (15) is the allowed range for the values of the design variables with an upper limit $x_i^u, i = 1...r$ and a lower limit $x_i^l, i = 1...r$ introduced to avoid numerical problems.

The optimization problem shown is difficult to solve due to its nonlinearity. Therefore, it is divided into two subproblems that are iterated stepwise one after the other to enable an efficient solution of the problem. A run of both subproblems is called an iteration step s. The detailed description of the two subproblems can be found in [6]. The optimization proceeds as follows: first, a starting vector for the design variable $\mathbf{x}_0$ is given. With this initial value, in subproblem 1, the orthonormal base $\bar{\boldsymbol{\Psi}} = [\bar{\boldsymbol{\varphi}}_1, \bar{\boldsymbol{\varphi}}_2, \dots, \bar{\boldsymbol{\varphi}}_m, \bar{\boldsymbol{\psi}}_1, \bar{\boldsymbol{\psi}}_2, \dots, \bar{\boldsymbol{\psi}}_{q-m}]$ for a $\bar{\mathbf{K}}(\mathbf{x}_0)$ seen as constant is computed and then expanded to $\boldsymbol{\Psi}$ on all p DoFs. The orthonormal base is an approximation to the eigenmodes of $\bar{\mathbf{K}}(\mathbf{x}_0)$, where the desired eigenmodes $\bar{\boldsymbol{\varphi}}_j,\ j = 1...m$ are assumed to be the first eigenmodes and all undesired modes $\bar{\boldsymbol{\psi}}_j,\ j = 1...q-m$ are calculated. The expanded orthonormal base then serves as input to the second subproblem, where the orthonormal base is seen to be constant and $\mathbf{K}(\mathbf{x})$ is varied. This solves the following optimization problem for the uncondensed stiffness matrix for the current iteration step s:

$$\max f(\mathbf{x}) = \sum_{j=1}^{l} \omega_j \, \boldsymbol{\psi}_j^T \, \mathbf{K}(\mathbf{x}) \, \boldsymbol{\psi}_j \tag{16}$$

s.t.:

$$g_i(\mathbf{x}) = \boldsymbol{\varphi}_i^T \mathbf{K} \boldsymbol{\varphi}_i - 2\mu \leq 0, i = 1 \dots m \tag{17}$$

$$h_1(\mathbf{x}) \dots h_{\binom{m}{2}}(\mathbf{x}) = \boldsymbol{\varphi}_i^T \mathbf{K} \boldsymbol{\varphi}_j = 0,\ i \neq j,\ i = 1 \dots m,\ j = 1 \dots m \tag{18}$$

$$m(\mathbf{x}) = \sum_{e=1}^{m} \frac{x_{e0}^{1/\eta}}{x_{e0}} x_e - mV \leq 0 \tag{19}$$

$$x_e^l \leq x_e \leq x_e^u,\ e = 1...m \tag{20}$$

The weighting factors are determined as follows:

$$\omega_j(s) = \frac{(\boldsymbol{\psi}_j^T \, \mathbf{K}(\mathbf{x}_0(s)) \, \boldsymbol{\psi}_j)^{-1}}{\sum_{j1=1}^{l1} (\boldsymbol{\psi}_{j1}^T \, \mathbf{K}(\mathbf{x}_0(s)) \, \boldsymbol{\psi}_{j1})^{-1}}, j = 1...l \tag{21}$$

Equation (16) is a substitude expression for the secondary stiffness that is maximized. For stability reasons, a number of l undesired modes are integrated into the objective function,

weighted equally for each iteration step. The associated weighting factors are calculated using equation (21). Equation (17) corresponds to equation (13), reformulated for the unconstrained problem. The optimization result is greatly improved by using equation (18). For the problem to be solved efficiently, it is necessary to linearize the volume constraint (14) to (19) using the starting vector for the design variables for the current iteration step $\mathbf{x}_0(s)$ [13]. Due to the finite elements used, the well-known checkerboard patterns may occur during optimization [14]. This problem can be avoided for example by using filter algorithms like the density filter [15]. This computes filtered design variables $\tilde{\mathbf{x}}(s)$ from the optimized design variables $\mathbf{x}(s)$ depending on a filter radius r_{min}. In order for the procedure to converge, it is now additionally necessary to constrain the change of the design variables between the iteration steps. Therefore, the vector of the filtered design variables $\tilde{\mathbf{x}}(s)$ is not used as the starting value for the next iteration step $\mathbf{x}_0(s+1)$, but it is calculated as a factor κ weighted sum between the start vector for the design variables for the current iteration step $\mathbf{x}_0(s)$ and the vector for the design variables $\tilde{\mathbf{x}}(s)$ calculated from the filtered ones in the current iteration:

$$\mathbf{x}_0(s+1) = \kappa \mathbf{x}_0(s) + (1-\kappa)\tilde{\mathbf{x}}(s) \tag{22}$$

For the stability of the optimization it is important to choose the factor κ as close to 1 as possible. The described procedure is now run through until convergence is reached.

3 OPTIMIZATION OF THE STIFFNESS-CONDITIONED FEATHER KEY

In practice, the feather key to be optimized has three-dimensional boundary conditions due to the load in shear. So far, however, the modal approach has been applied exclusively to planar structures. Although an extension is easily possible, the time required for optimization increases considerably. Therefore, the feather key is optimized in a simplified planar way. A shaft diameter of $d = 40$ mm is assumed for the sensor-integrating feather key. In DIN 6885 [3], the height of the feather key is set to $h = 8$ mm and the width of the feather key to $b = 12$ mm for this shaft diameter. The length must meet the requirement $l_{PF} \leq 1.3d$. We choose the limiting case $l_{PF} = 1.3d$ for the feather key length. A feather key shape b is chosen due to better sensor integrability. The cross section to be optimized, is marked in Figure 2 (a). It is assumed that the feather key is clamped on one side. On the opposite side, the desired deformation modes are applied to the active DoFs. These are the y-displacements of the points marked in red. In addition, the x-displacements of the center point are set to zero for both desired deformation modes. In the cross-section to be optimized, areas are defined where the stiffnesses of the finite elements are part of the overall stiffness matrix, but are not integrated into the optimization (fixed elements). In the white area, the material is then distributed during the optimization. Normally, CMs with selective compliance should have high selectivities. To achieve this, a low limit for the primary stiffnesses is selected. However, the feather key is to transmit torques in addition to the measuring task, which is why a high primary stiffness is desirable. If the feather key is optimized, the stiffness is reduced and thus the load carrying capacity to the full feather key is weakened in order to achieve the optimization goals. A compromise must therefore be found between the two competing requirements of a high selectivity and a high stiffness. If de-

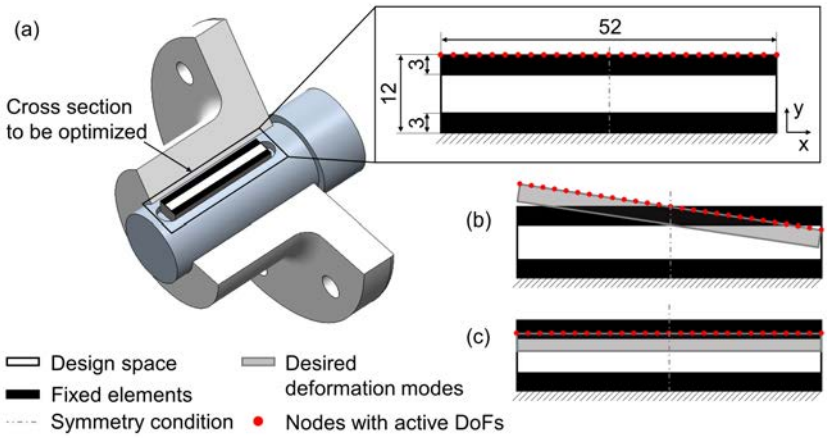

Figure 2: (a) Location, dimensions and boundary conditions of the cross section of the feather key to be optimized, (b) First desired eigenmode, (c) Second desired eigenmode

sired deformation modes are chosen that can be addressed as well as possible with the expected pressure distributions, the selectivity can be low and the existing deformation still be composed approximately of the desired deformation modes. As shown in Figure 1, we expect parabolic pressure distributions. Important parameters here are mainly the stretching, as well as the displacement of the parabola vertical to the surface with the active DoFs. These two parameters can be represented with the desired eigenmodes shown in Figure 2(b) and (c) (pseudo-mobility two). Due to the symmetry of the two desired deformation modes, a symmetry condition can be introduced. Here, a symmetry of the structure is enforced during the optimization instead of the classical symmetry condition known from the finite element method. The limit for the primary stiffnesses $\mu = 2000$ was chosen such that sufficiently high selectivities could still be achieved. This was determined by numerical tests. The other parameters for optimization were chosen as follows: $l = 26, V = 0.95, r_{min} = 2.9, \kappa = 0.99, \eta = 3, x_i^l = 0.0001, x_i^u = 1$,. The material properties were set to $E = 210$ GPa and $\nu = 0.3$ for Young's modulus and Poisson's ratio, respectively. In addition, the optimization result depends on the chosen starting vector of the design variable $\mathbf{x}_0$. Optimizations were started from different starting vectors and then the structure with the highest selectivity was chosen for practical implementation.

The structure with the highest selectivity ($S = 1.93$) and its existing first two eigenmodes are shown in Figure 3. The first two eigenmodes of this structure (Figure 3 (b) and (c)) are similar to the desired first eigenmodes, but there is more deviation than in previous optimizations of other CMs with multiple pseudo-mobility [6] due to the high primary stiffness required. However, the deviation of the eigenmodes is negligible if the kinematic instead of the desired eigenmodes are included in the further considerations. Above all, it is important that in realistic simulations the deformations at the surface of the feather key with the active DoFs are approximately composed of these two modes. If this is achieved, the deformation of the entire feather key can be determined using two strain gauges.

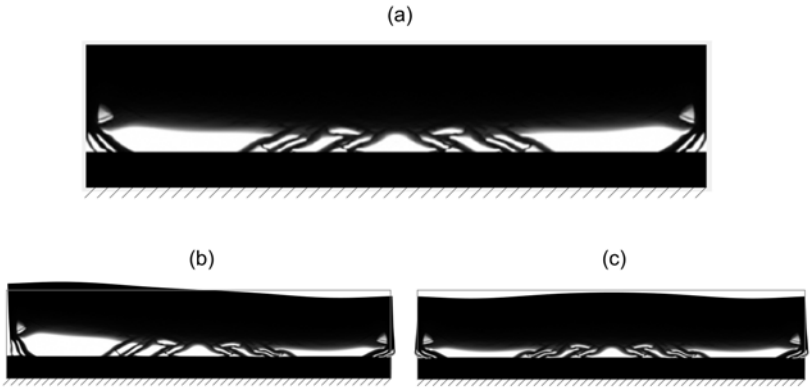

Figure 3: (a) Optimization result, (b) First kinematic eigenmode, (c) Second kinematic eigenmode

4 NUMERICAL VALIDATION

For validation, the optimized structure is interpreted as a CAD part (Figure 4 (a)). In doing so, the structure can be greatly simplified while maintaining the stiffness properties imposed in the optimization. The behavior of this structure is simulated under realistic boundary conditions using the commercial program ABAQUS. Here, the shaft and hub are connected by two stiffness-conditioned feather keys arranged at an angle of $180°$. The arrangement of the feather keys was chosen in such a way to prevent asymmetric load distribution due to the tilting behavior of the feather keys. Two models were made from the basically same components. The chosen dimensions are shown in Figure 4. The difference between the models is that in the second model, compared to the first, the hub was rotated to change the distribution of pressure on the feather key. The model shown in Figure 4(b) will be referred to as model 1 and the model shown in Figure 4(c) will be referred to as model 2 in the following. The dimensions of the modeled feather keys correspond to the dimensions from the optimization in Figure 2. In both models, the hub is fixed to the cylindrical face of the hub flange and a torque M_t is applied to the shaft. In the elastic simulation, $E = 210$ GPa and $\nu = 0.3$ are assumed for all components. The feather key is meshed using 8-node elements with incompatible modes. For the regions of the other components directly adjacent to the feather keys, the same element type is used. For remaining areas, 8-node elements with reduced integration are used. It is assumed that ideally joined components exist. Therefore, oversizes between shaft and hub and between notches and feather key are not considered in the simulation. In the simulation, the three substeps frictionless finding of the contact surfaces, activation of the friction value $\mu = 0.2$ and application of the torque $M_t = 1000$ Nm are run through. The surface contact was modeled using the pure-penalty method.

The simulated deformations of the feather keys for both models are shown in Figure 5. For each model, the deformation of one of the two feather keys was evaluated, since the deformations are the same for both feather keys of the double feather key connection. When the shaft

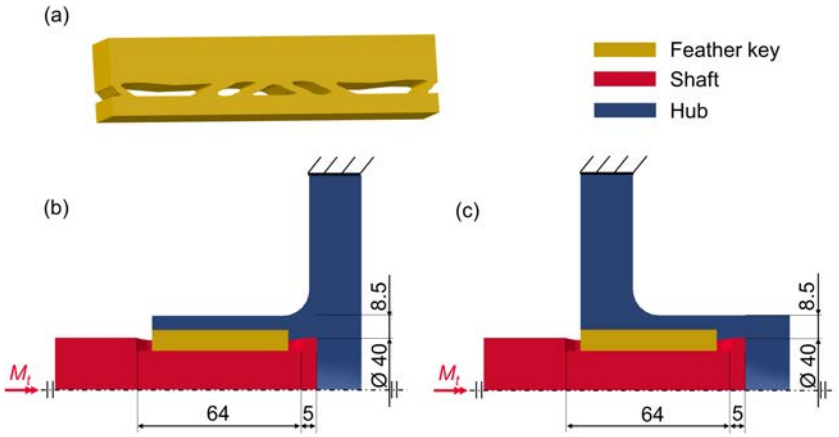

Figure 4: (a) Interpreted stiffness-conditioned feather key, (b) Model 1 (c) Model 2.

is torqued by the applied moment, the feather keys experience a rigid body displacement. This effect must be eliminated, since only the local deformation of the feather keys is of interest. Therefore, a co-moving coordinate system is applied to each of the feather keys (see Figure 5), which is used as a reference for the evaluated displacements. In relation to this coordinate system, the x-displacement of the line marked in red is evaluated. This line was chosen for the evaluation, because on the one hand it is conveniently located for the later setup of the measurement technique and on the other hand it is as far away as possible from occurring shear effects.

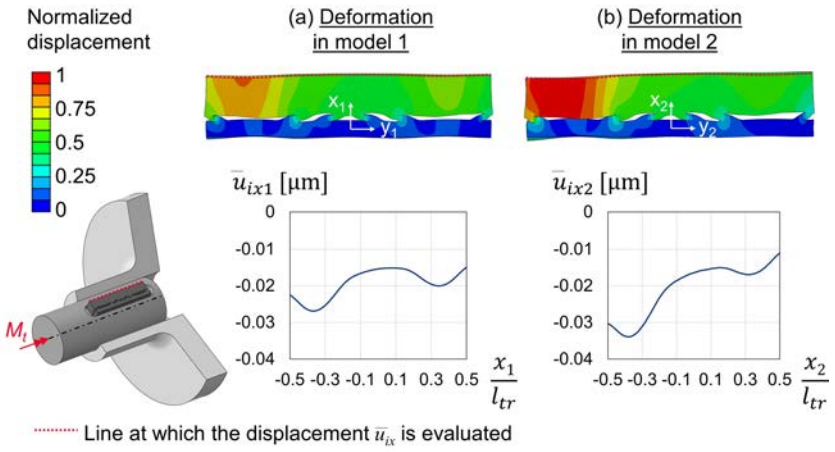

Figure 5: Results of simulations with realistic boundary conditions, top: Deformations of the feather keys, bottom: Plot of displacement in relation to the local coordinate system on the feather key for (a) Model 1 and (b) Model 2

As explained earlier, the objective of the stiffness conditioning of the feather key is to ensure that the displacements are composed of the two kinematic eigenmodes as well as possible. For

verification, the dot product of the normalized displacement vector $\bar{\mathbf{u}}$ of the displacements of the nodal points lying on the evaluation line can be formed with the kinematic eigenmodes. This calculation yields for model 1 $a_1 = (\bar{\mathbf{u}}_{x1} \cdot \bar{\boldsymbol{\chi}}_1)^2 = 0.016$ and $b_1 = (\bar{\mathbf{u}}_{x1} \cdot \bar{\boldsymbol{\chi}}_2)^2 = 0.924$. The results for model 2 are $a_2 = (\bar{\mathbf{u}}_{x2} \cdot \bar{\boldsymbol{\chi}}_1)^2 = 0.081$ and $b_2 = (\bar{\mathbf{u}}_{x2} \cdot \bar{\boldsymbol{\chi}}_2)^2 = 0.864$.

A displacement is completely composed of the kinematic eigenmodes if the sum of the associated squared dot products ($a_i + b_i, i = 1...2$) equals one. The dot products must be squared because they were previously normalized with formula (5). It can be seen that approximately 94 % of the shift in both models is composed of the two desired eigenmodes. Thus, the complex deformation of the feather key could be simplified by stiffness conditioning to a deformation that can be approximately expressed as a linear combination of two known kinematic eigenmodes. This means that the deformation can be determined with two strain gauges if they are placed close to the evaluated lines so that the influence of shear can be neglected.

5 CONCLUSION

It was shown that the already known modal approach is also suitable for the optimization of a stiffness-conditioned feather key. The optimization goal is that the deformation of the feather key in certain DoFs is approximately composed of a linear combination of two kinematic eigenmodes, independent of the applied pressure distribution. This property makes it possible to accurately determine the deformation of the feather key with two strain gauges. As a result, the transmitted torque can be calculated with little effort for different pressure distributions. Although the feather key was optimized under planar boundary conditions, it was shown that the desired properties can also be approximately ensured under realistic three-dimensional boundary conditions.

In the future, it is necessary to check whether the achieved approximation of the deformation to a linear combination of the two desired eigenmodes is sufficient for the measurement with two strain gauges. If the achieved approximation is not sufficient, a new optimization with either modified planar boundary conditions or $m = 3$ has to be performed. Additionally, sensor positioning and practical tests have to be performed to validate the calculation.

Acknowledgements

Funded by the Deutsche Forschungsgemeinschaft (DFG, German Research Foundation) – SPP 2305 ‘Sensor-integrated machine elements’ (project number 466657550).

REFERENCES

[1] A. Harder, M. Hausmann, B. Kraus, E. Kirchner, and A. Hasse, “Sensory Utilizable Design Elements: Classifications, Applications and Challenges,” *Appl. Mech.*, vol. 3, no. 1, pp. 160–173, 2022.

[2] S. Vogel, G. Martin, T. Schirra, and E. Kirchner, “Robust design for mechatronic machine elements - how robust designenables the application of mechatronic shaft-hub connection,” in *15th International Design Conference*, 2018, pp. 3033–3040.

[3] Deutsches Institut für Normung e.V., *DIN 6885: Mitnehmerverbindungen Ohne Anzug; Paßfedern, Nuten, Hohe Form*. Berlin: Beuth, 1968.

[4] P. Groche and T. Traub, "Passfeder zur Bestimmung des übertragenen Drehmomentes," Germany Patent Patent, DE102 016 110 577A1, 2019.

[5] A. Bader, "Verfahren zur Detektion einer Überlastung einer Welle-Nabe-Verbindung," Germany Patent, 2011.

[6] S. Seltmann, L. F. Campanile, and A. Hasse, "Topology-optimization based design of multi-degree-of-freedom compliant mechanisms (mechanisms with multiple pseudo-mobility)," *J. Intell. Mater. Syst. Struct.*, pp. 609–628, 2022.

[7] S. R. Deepak, M. Dinesh, D. K. Sahu, and G. K. Ananthasuresh, "A Comparative Study of the Formulations and Benchmark Problems for the Topology Optimization of Compliant Mechanisms," *J. Mech. Robot.*, vol. 1, no. 1, p. 011003, 2009.

[8] N. F. Wang and K. Tai, "Design of 2-DOF Compliant Mechanisms to Form Grip-and-Move Manipulators for 2D Workspace," *J. Mech. Des.*, vol. 132, no. 3, p. 031007, 2010.

[9] B. Zhu, Q. Chen, M. Jin, and X. Zhang, "Design of fully decoupled compliant mechanisms with multiple degrees of freedom using topology optimization," *Mech. Mach. Theory*, vol. 126, pp. 413–428, 2018.

[10] J. Zhan and X. Zhang, "Topology optimization of multiple inputs and multiple outputs compliant mechanisms using the ground structure approach," in *2010 2nd Int. Conf. Ind. Mechatron. Autom.*, vol. 1. IEEE, 2010, pp. 20–24.

[11] C. Alonso, R. Ansola, and O. M. Querin, "Topology synthesis of Multi-Input–Multi-Output compliant mechanisms," *Adv. Eng. Software*, vol. 76, pp. 125–132, 2014.

[12] A. Hasse and L. F. Campanile, "Design of compliant mechanisms with selective compliance," *Smart Mater. Struct.*, vol. 18, no. 11, p. 115016, 2009.

[13] S. Seltmann and A. Hasse, "Topology optimization of compliant mechanisms with distributed compliance (hinge-free compliant mechanisms) by using stiffness and adaptive volume constraints instead of stress constraints," *Mech. Mach. Theory*, vol. 180, p. 105133, 2023.

[14] M. P. Bendsøe and O. Sigmund, in *Topology Optimization: Theory, Methods, and Applications*. Berlin ; New York: Springer, 2003, pp. 4–7.

[15] T. E. Bruns and D. A. Tortorelli, "Topology optimization of non-linear elastic structures and compliant mechanisms," *Comput. Methods Appl. Mech. Eng.*, vol. 190, no. 26-27, pp. 3443–3459, 2001.